Food Chemistry: X 25 (2025) 102177

Contents lists available at ScienceDirect

Food Chemistry: X

journal homepage: www.sciencedirect.com/journal/food-chemistry-x

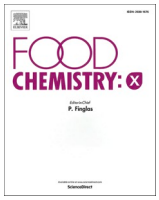

Preparation of flavonoids from *Amomum tsaoko* and evaluation of their antioxidant and α-glucosidase inhibitory activities

Zelin Huang [a,b,c,1], Yan Zhao [d,1], Weixing Yang [b], Lu Lang [b], Jun Sheng [c], Yang Tian [a,c,**], Xiaoyu Gao [a,b,c,*]

[a] Yunnan Key Laboratory of Precision Nutrition and Personalized Food Manufacturing, Yunnan Agricultural University, Kunming 650201, China
[b] College of Food Science and Technology, Yunnan Agricultural University, Kunming 650201, China
[c] Engineering Research Center of Development and Utilization of Food and Drug Homologous Resources, Ministry of Education, Yunnan Agricultural University, Kunming 650201, China
[d] Division of Science and Technology, Yunnan Agricultural University, Kunming 650201, China

ARTICLE INFO

Keywords:
Flavonoids
Ultrasound-assisted extraction
Macroporous resin
Amomum tsaoko
Widely targeted metabolomics

ABSTRACT

Amomum tsaoko is an important homologous medicinal and food plant, and its fruit is rich in flavonoids. However, few studies have reported the preparation and bioactivity of flavonoids in *A. tsaoko* (ATF). In this study, the optimal conditions for ultrasound-assisted extraction of ATF were identified through response surface optimization. HPD300 was identified as the best resin for the purification of ATF, as it exhibited a Freundlich model-conformative adsorption isotherm. Among the different concentrations of ethanol, 20 % and 30 % resulted in higher flavonoid purity (>90 %) and stronger antioxidant and α-glucosidase inhibition activities. A widely targeted metabolomics assay revealed that the relative abundance of flavonoids in a mixture of 20 % and 30 % ethanol eluates was greater than 73 %, which mainly contained (+)-epicatechin, isoquercitrin, astragalin kaempferol-3-O-rutinoside, and procyanidin B2. These findings provide a theoretical basis for the in-depth development and potential use of ATF in the functional food, cosmetic and pharmaceutical industries.

1. Introduction

Amomum tsaoko Crevost et Lemarie is a perennial evergreen clumping herb in the genus *Cardamom* of the ginger family (Zhang et al., 2022). It produces fruits with a special rich spicy flavor that can remove fishy and dingy flavors and increase appetite. *A. tsaoko* fructus (AT) is a Chinese food flavoring "one of the five spices". Notably, AT is also among the most prevalent species in China's medicinal and food homologous resources. It is included in the Chinese Pharmacopoeia and is known to have several pharmacological effects, including the promotion of warming in the body, strengthening of the stomach, elimination of food, and regulation of breathing (Zhang et al., 2014). The distribution of AT is primarily concentrated in the provinces of Yunnan, Guangxi, and Guizhou in China (Wu et al., 2023). However, the AT industry is currently characterized by a relatively short industrial chain and a lack of deep processing, which results in the production of low-value-added products. The vast majority of ATs are used only as spices, and there is a notable absence of research and development on the medicinal value of ATs.

In recent years, with the gradual deepening of research on AT, certain progress has been made in the study of its chemical composition and pharmacological activity. To date, scientists have isolated more than 300 compounds from AT, which can be categorized into flavonoids, terpenoids, phenylpropanoids, diphenylheptanes, aromatic substances, and others (Cai et al., 2021; Yang et al., 2022). Among these, flavonoids are the main components of AT, which have been demonstrated to function as excellent antioxidants, effectively scavenging free radicals associated with a variety of diseases (Andrade et al., 2018). Additionally, they have been shown to significantly inhibit the activity of α-glucosidase, which plays a role in regulating blood glucose levels and thus preventing diabetes mellitus (Li, Yang, et al., 2023). These findings underscore the importance of isolating, extracting, and evaluating the

* Corresponding author.
** Corresponding author at: Yunnan Key Laboratory of Precision Nutrition and Personalized Food Manufacturing, Yunnan Agricultural University, Kunming 650201, China.
E-mail addresses: tianyang@ynau.edu.cn (Y. Tian), 2018014@ynau.edu.cn (X. Gao).
[1] Contributed equally to this work.

https://doi.org/10.1016/j.fochx.2025.102177
Received 23 July 2024; Received in revised form 5 January 2025; Accepted 11 January 2025
Available online 13 January 2025

functional properties of flavonoids in AT for the comprehensive utilization of AT resources.

The conventional extraction techniques for flavonoids include immersion, decoction, Soxhlet extraction, and other methods. However, these approaches are unable to meet the increasing demand for the separation and extraction of flavonoids (Chávez-González et al., 2020). Ultrasonic-assisted extraction (UAE) is based on the solution extraction method, whereby the cavitation effect generated by ultrasonication is harnessed to create cavitation air cannons within the extraction solution. Detonation of the shockwaves results in disintegration of the plant cell wall, thereby increasing the solubility of the target components (Qin et al., 2023). In practical applications, UAE has the potential to extract active compounds effectively from spices while preserving the structural integrity of flavonoids (Teng et al., 2019). However, the greater the degree of substance fragmentation resulting from the stronger the cavitation effect of ultrasound, the greater is the potential for precipitation of some impurities, which may affect the efficiency of flavonoid extraction (Tian et al., 2019). Therefore, it is necessary to optimize the UAE conditions rationally to achieve the optimal flavonoid yield. Macroporous resins (MRs) are widely utilized, cost-effective, and environmentally benign purification methods for industrial production. MR has been applied to the isolation and purification of a variety of active ingredients, including plant flavonoid compounds (Wang et al., 2022). However, studies on the isolation of flavonoids from AT using MRs in conjunction with UAE are scarce. The search for an optimal method for the preparation of AT flavonoids is highly valuable for the advancement and utilization of AT resources.

In this study, we employed a combined UAE and MR method for the preparation of total flavonoids from AT. The optimal preparation process conditions were determined, and different ethanol concentrations with high flavonoid contents were obtained. The antioxidant and α-glucosidase inhibitory activities of the elutions were subsequently evaluated in vitro, and the chemical composition of the highly active elutions was elucidated through the use of a widely targeted metabolomics assay. These findings may provide a foundation for future functional and pharmacological studies and the comprehensive utilization of AT.

2. Materials and methods

2.1. Chemicals and materials

Dried AT was procured from Gongshan County, Yunnan Province, where any damaged or suboptimal specimens were excluded. The AT was then subjected to a crushing process in our lab and subsequently passed through a 40-mesh sieve. The standard for rutin was obtained from Dalian Meilun Biotech Co., Ltd. (Dalian, China). All MRs were procured from Beijing Solarbio Science & Technology Co., Ltd. Table S1 presents the physical properties of all MRs in this work.

UP H_2O was prepared using an ultrapure water system (Purifier, Shanghai, China), and all other chemicals and solvents employed in this work were of analytical grade.

2.2. Optimization of the UAE process for extracting flavonoids from AT

2.2.1. Preparation of the ethanol extract of AT

The AT powder (40-mesh) was weighed and combined with a specified volume of an ethanol solution, which was then soaked and extracted using ultrasonic waves. The extract was then centrifuged at 4000 rpm for 15 min, after which the volume of the supernatant was adjusted to the original volume to obtain the ethanol extract of AT (ATEE).

2.2.2. Determination of flavonoid contents in extracts

The colorimetric method of $NaNO_3$-$Al(NO_3)_3$-NaOH (Lin et al., 2014) was employed for the determination of flavonoids in different extracts. A standard curve was constructed using rutin as the standard, resulting in the linear regression eq. $Y = 6.6827\times + 0.0105$, $R^2 = 0.9993$. The yield of flavonoids in the AT extracts was then calculated according to eq. (1).

$$Y(\%) = \frac{N \times C \times V}{M \times 1000} \times 100\% \quad (1)$$

Y is the flavonoid yield (%); C is the concentration of flavonoids (mg/mL), which is calculated according to the standard curve equation; N is the dilution of extracts; V is the volume of determinate extracts (mL); and M is the mass of AT powder (g).

2.2.3. Single-factor experiments

The flavonoids were extracted by soaking AT powder in 60 % ethanol at a material–liquid ratio of 1:25 (*w/v*), and the effects of soaking time (0.5, 1.0, 1.5, 2.5, 4.5, 8.5, 12, and 24 h) on the extraction of flavonoids from AT were investigated. Once the optimal soaking time was identified, a series of experiments were conducted to investigate the impact of various factors on the extraction rate of flavonoids in AT (ATF). These factors included the ethanol concentration (40 %, 50 %, 60 %, 70 %, 80 %), solid–liquid ratio (1:15, 1:20, 1:25, 1:30, 1:35, 1:40, 1:45, 1:50), ultrasonic power (120, 140, 160, 180, 200 W), ultrasonication time (10, 20, 30, 40, 50, 60 min), and ultrasonication temperature (25, 35, 45, 55, 65, 75 °C), with each factor being investigated sequentially.

2.2.4. Response surface optimization experiments

A Box–Behnken response surface design was employed to optimize the extraction conditions for ATF. The material–liquid ratio (A), ultrasonic power (B), ultrasonic time (C), and ultrasonic temperature (D) were investigated for their effects on the ATF (Table 1).

2.3. Process optimization of ATF purification by MRs

2.3.1. Pretreatment of MRs

All MRs were first soaked in 95 % ethanol for 12 h, followed by washing with UP H_2O until they were odorless; subsequently, all MRs were soaked in 5 % sodium hydroxide for 4 h, followed by washing with UP H_2O until they were neutral; finally, they were soaked in 5 % hydrochloric acid for 4 h and washed with UP water until they were neutral. The activated MRs were immersed in UP H_2O and maintained in reserve.

2.3.2. Screening of MRs

Adsorption/desorption tests were conducted on ten MRs. The activated MRs were accurately weighed and placed in a 250 mL conical flask, to which 100 mL of ATEE was added. The conical flask was then shaken for 24 h at 25 °C and 140 r/min. After adsorption equilibrium was reached, all the MRs were retained and washed thoroughly with UP water, and then 100 mL of 80 % ethanol was added and desorbed by shaking for 24 h (25 °C, 140 r/min). The adsorption rate, adsorption capacity, desorption rate, and desorption capacity were calculated using eqs. (2), (3), (4), and (5), respectively.

$$\text{Adsorption rate}: A(\%) = \frac{C_0V_0 - C_eV_e}{C_0V_0} \times 100\% \quad (2)$$

$$\text{Adsorption capacity}: Q_e = \frac{C_0V_0 - C_eV_e}{m} \quad (3)$$

Table 1
Factors and levels employed in the Box–Behnken response surface design.

Levels	Factors			
	A: Solid–liquid ratio (w/v)	B:Ultrasonic power (W)	C:Ultrasonic time (min)	D:Ultrasonic temperature (°C)
−1	1:30	160	40	60
0	1:35	180	50	65
1	1:40	200	60	70

$$\text{Desorption rate}: D(\%) = \frac{C_d V_d}{C_0 V_0 - C_e V_e} \times 100\% \quad (4)$$

$$\text{Desorption capacity}: Q_d(\%) = \frac{C_d V_d}{m} \quad (5)$$

The adsorption and desorption rates, designated A and D (%), respectively, are dependent upon the concentrations of ATF before adsorption, at adsorption equilibrium, and in the desorption solution, designated C_0, C_e, and C_d (mg/mL), respectively; V_0, V_e, and V_d (mL) represent the volumes of the solution prior to adsorption, at the time of adsorption, and following desorption, respectively. Q_e and Q_d (mg/g) represent the equilibrium adsorption and desorption amounts, respectively; finally, m (g) denotes the wet weight of the MRs.

2.3.3. Adsorption kinetics

ATEE containing 2.0 mg/mL flavonoids was prepared and mixed with 5 g of pretreated MRs. The adsorption capacity of the MRs was determined at different adsorption times by shaking at 140 rpm at 25 °C. The adsorption processes of MRs were analyzed using the pseudo-first-order, pseudo-second-order, and intraparticle diffusion model, respectively.

$$\text{Pseudo}-\text{first}-\text{order kinetic model}: ln(Q_e - Q_t) = lnQ_e - k_1 t \quad (6)$$

$$\text{Pseudo}-\text{second}-\text{order kinetic model}: \frac{t}{Q_t} = \frac{t}{Q_e} + \frac{1}{k_2 Q_e} \quad (7)$$

$$\text{Intraparticle diffusion model}: Q_t = k_3 t^{\frac{1}{2}} + M \quad (8)$$

Q_e and Q_t represent the adsorption capacities at equilibrium and at time t, respectively; K_1, K_2, and K_3 denote the rate constants for the pseudo-first-order model, pseudo-second-order model, and intraparticle diffusion model, respectively. M denotes the constant in the intraparticle diffusion model.

2.3.4. Adsorption isotherms

ATEE with varying concentrations (0.4–3.2 mg/mL) was prepared and combined with 5 g of MRs. Adsorption was performed by shaking at 140 rpm at 25, 35, and 45 °C, respectively, and the adsorption capacity of the MRs was determined using the Freundlich and Langmuir models.

$$\text{Langmuir model}: \frac{C_e}{Q_e} = \frac{C_e}{Q_m} + \frac{1}{k_L Q_m} \quad (9)$$

$$\text{Freundlich model}: lnQ_e = \frac{1}{n} lnC_e + lnk_F \quad (10)$$

where Q_m (mg/g) is the theoretical maximum adsorption capacity; k_L (mL/mg) is the Langmuir model constant; n and k_F are the Freundlich equation constants; and k_F reflects the adsorption capacity.

2.3.5. Optimization of process conditions for purification of ATF by screened MR

A specific concentration of ATEE was prepared, and the pH was adjusted by the addition of either an HCl solution (1 mol/L) or a NaOH solution (1 mol/L). This procedure was followed by the addition of 5 g of resin and shaking for 8 h at 25 °C with a shaking speed of 140 rpm. Once equilibrium had been reached, the resin was loaded onto the column in a wet state and poured into solutions of ethanol at concentrations ranging from 10 % to 100 %. Each solution was then eluted until the solution became colorless. The volume of elution at each ethanol concentration was recorded, and the ATF content in the elution solution at each concentration was determined.

2.4. In vitro evaluation of bioactivities

2.4.1. Antioxidant activity

FRAP, DPPH, ABTS and hydroxyl radical-scavenging assays were used to determine ATEE before purification, as were the ATF fractions obtained by elution with ethanol at 10 % to 50 % concentrations according to Vo et al. (2023) and Maduwanthi and Marapana (2021). Vc was also used as a positive control.

2.4.2. α-Glucosidase activity inhibition assay

An α-glucosidase activity inhibition assay was performed to determine ATEE before purification, and ATF fractions were obtained by elution with 10 % to 50 % ethanol according to the methods of Dao et al. (2021). Acarbose was also used as a positive control.

2.5. Phytochemical composition determination using widely targeted metabolomics

The lyophilized powders of the 20 % and 30 % ethanol elutions were completely mixed, and the flavonoid content was determined using the $NaNO_3$-$Al(NO_3)_3$-NaOH colorimetric method and submitted to Shanghai Biotree Biomedical Science and Technology Co. Ltd. for widely targeted metabolomics analysis. Briefly, a total of 10 mg of lyophilized ATF powder was combined in a centrifuge tube with 2 small steel balls and 500 μL of extract (methanol:water, volume ratio of 1:2). After a series of pretreatment steps, the mixture was passed through an EXIONLCS system (SCIEX) for high-performance liquid chromatography (HPLC) to separate the target components. A Waters UPLC liquid chromatography column (Acquity UPLC HSS T3, 2.1 mm * 100 mm, 1.8 μm) was utilized. Liquid chromatographic phase A was an aqueous solution containing 0.1 % formic acid, while phase B was acetonitrile. A Sciex QTrap 6500+ (Sciex Technologies) was used for assay development. SCIEX Analyst Work Station software (version 1.6.3) was used for MRM data acquisition and processing. MS raw data files (wiff) were converted to TXT format using the MS Converter. An in-house R program and database were used for peak detection and annotation.

2.6. Statistical analysis

The data are expressed as the means ± standard errors of the means (SEMs). Analysis of variance was conducted using the statistical software package SPSS 26.0 (SPSS Inc., Chicago, IL, USA). Statistical analysis of the results was conducted using analysis of variance (ANOVA) with Duncan's test. The statistical significance of the differences between the means of each factor was determined at $P < 0.05$. The Box–Behnken response surface design was conducted using Design Expert 8.0.6 software (StatEase®, Minneapolis, USA). GraphPad Prism 8.0 software was used for plotting and linear regression analysis, with the objective of obtaining kinetic-related parameters and IC_{50} values.

3. Results and discussion

3.1. Optimization of the ATF extraction conditions

3.1.1. Single-factor experiments

The results of single-factor experiments for ATF extraction are shown in Fig. 1. As the soaking time increased, the flavonoids continuously precipitated, and the flavonoid content in the soaking solution tended to stabilize after 12 h of soaking (Fig. 1A). Therefore, a soaking time of 12 h was used. As illustrated in Fig. 1B and C, the flavonoid yields initially increased but then decreased as the ethanol concentration and solid–liquid ratio increased. The highest flavonoid yield was obtained when the ethanol concentration was 60 % and the solid–liquid ratio was 1:35 (*w/v*), with yields of 2.91 % and 3.11 %, respectively. An appropriate ethanol concentration and solid-to-liquid ratio may provide conditions such as appropriate polarity and an opportunity for solvent contact for

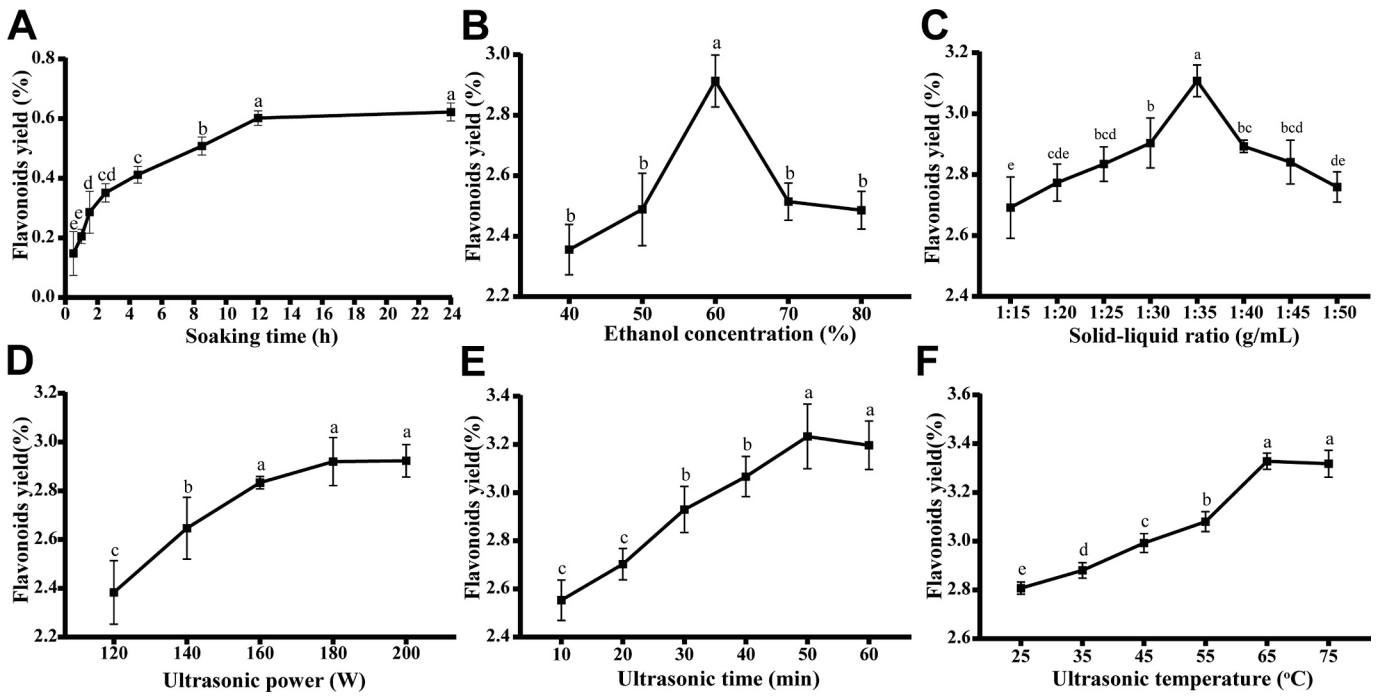

Fig. 1. Effects of a single factor on the flavonoid yield from AT.

the dissolution of more flavonoids from AT powder (Liao et al., 2021).

The ultrasound parameters also had a notable influence on the flavonoid yield. The ATF yield increased with increasing ultrasonic power, ultrasonication time and ultrasonication temperature. However, when these ultrasonic parameters reached a certain threshold, the yield of flavonoids tended to stabilize following an increase, or even decrease (Figs. 1D to 1F). The underlying cause of this phenomenon might be that when these ultrasound parameters were below the threshold, an increase in power resulted in a stronger cavitation effect, which in turn led to faster breakdown and precipitation of the flavonoids. Moreover, an increase in temperature also facilitated the diffusion of flavonoids, whereas an increase in ultrasonication time was conducive to the accumulation of these molecules. However, when the threshold value was exceeded, the amount of flavonoids released and diffused into the solvent reached a maximum. Excessively high ultrasonic power, temperature and time generate excessive energy, which may result in the destruction or degradation of some flavonoids (Tian et al., 2019). Therefore, the optimized ATF extraction conditions obtained from the single factor experiments were an ethanol concentration of 60 %, a solid–liquid ratio of 1:35 (*w/v*), an ultrasonication power of 180 W, an ultrasonication time of 50 min, and an ultrasonication temperature of 65 °C.

(A) Soaking time, (B) ethanol concentration, (C) solid–liquid ratio, (D) ultrasonic power, (E) ultrasonic time and (F) ultrasonic temperature. The presence of different letters indicates that the observed differences are statistically significant ($P < 0.05$). Conversely, the absence of letters indicates that the observed differences are not statistically significant ($P > 0.05$).

3.1.2. Response surface optimization experiments

A multivariate quadratic regression model was developed using data from Table S2 to establish a regression model for the extraction process parameters. The regression equation is presented in eq. (12).

$$Y = 3.12 + 0.099A + 0.040B + 0.017C + 0.083D - 0.040AB + 0.022AC + 0.075CE + 0.090BCE - 0.12BD - 0.10CD - 0.067A^2 - 0.028B^2 - 0.20C^2 - 0.069D^2 \quad (12)$$

where Y, A, B, C and D denote the flavonoid yield (%), material–liquid ratio, ultrasonic power, ultrasonication time and ultrasonication temperature, respectively.

As shown in Table S3, the F value of the quadratic regression model was 22.55, with a *P* value of less than 0.01, indicating a highly significant level. The lack of fit was not significant ($P > 0.05$), and the results indicated that the regression equation was well fitted. Furthermore, the model showed a high degree of fit, with a decision coefficient of $R^2 = 0.9575$ and an adjusted decision coefficient of $R^2_{Adj} = 0.9151$. This observation indicated a strong correlation between the predicted and actual results, confirming the suitability of the model for analysis.

As illustrated in Fig. 2 and Fig. S1, the contours of AD, BC, BD, and CD were elliptical, indicating that the interaction between the two variables had a significant effect on the flavonoid yield (Wen, Zeng, et al., 2023). Moreover, the 3D response surfaces for A exhibited steeper slopes than those for B, C, and D (Figs. 2A to 2C). The B slope was steeper than the C slope (Fig. 2J), and the D slope was steeper than the B and C slops (Fig. 2K and L). In general, the influence order of each factor on the flavonoid yield was A > D > B > C.

(A) Solid–liquid ratio and ultrasonic power, (B) solid–liquid ratio and ultrasonic time, (C) solid–liquid ratio and ultrasonic temperature, (D) ultrasonic power and ultrasonic time, (E) ultrasonic power and ultrasonic temperature, and (F) ultrasonic time and ultrasonic temperature.

3.1.3. Model validation

Through response surface design optimization, the optimal process conditions for flavonoid extraction were identified as a material–liquid ratio of 1:38.08, an ultrasonic power of 163.23 W, an ultrasonic time of 46.51 min, and an ultrasonic temperature of 69.44 °C. These conditions yielded the highest predicted flavonoid yield, reaching 3.31 %. Considering the feasibility of practical operation, three validation tests were conducted under the following process conditions: a material–liquid ratio of 1:39 (*w/v*), an ultrasonic power of 160 W, an ultrasonic time of 47 min, and an ultrasonic temperature of 69 °C. The actual measured flavonoid yield was 3.33 %, which was in close agreement with the predicted value. These results indicated that the process conditions optimized by the response surface model were accurate and reliable. Additionally, the flavonoid content of the ultrasound extract

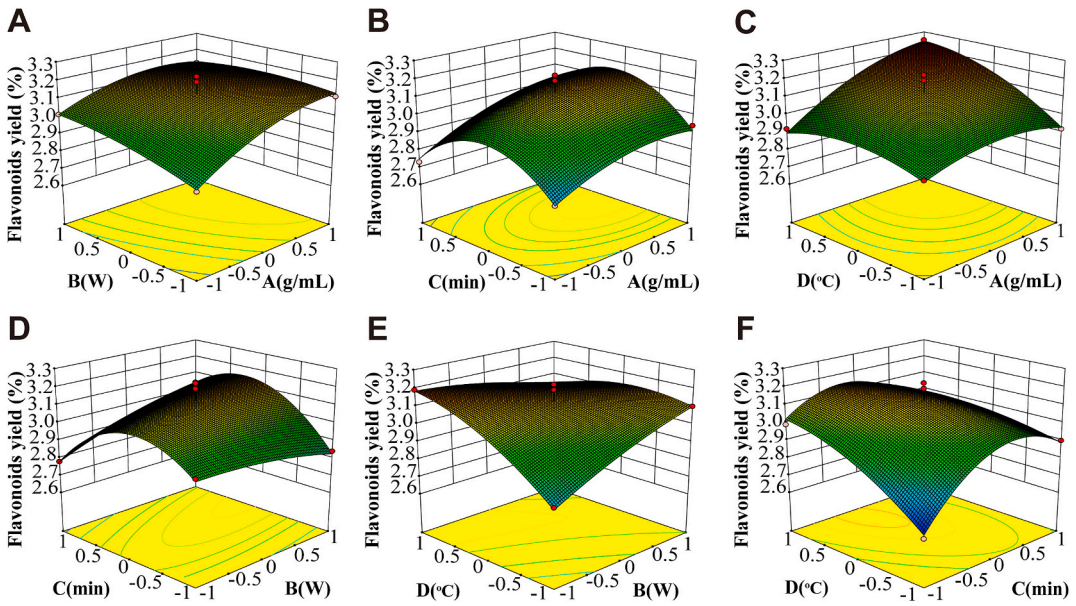

Fig. 2. The 3D response surface plots illustrating the influence of various parameters on flavonoid yield.

was determined to be 21.71 %. In previous studies, response surface methodology was employed to optimize the optimal extraction conditions for the ultrasound-assisted extraction of perilla leaf flavonoids (Li, Lin, et al., 2023) and *Murraya exotica* flavonoids (Wen, Liu, & Mai, 2023). The required ultrasound energy exceeded 200 W, the dosage of material and liquid was high, and the extraction rate was 1.0 % or less. However, in this study, the amount of ethanol used was conserved, the energy consumption was reduced, and the extraction efficiency was effectively improved to 3.33 %. These findings indicated that the ultrasonic extraction conditions employed effectively increased the flavonoid content.

3.2. Separation and purification of ATF by MRs

3.2.1. Selection of MRs

MRs are capable of reversibly adsorbing external organic matter, with the main driving forces being hydrogen bonding and van der Waals forces, and their adsorption performance is closely related to the specific surface area, pore size, and polarity (Li & Chase, 2010). As illustrated in Fig. 3, the adsorption/desorption capacities of the various MRs differed, with the less polar MRs exhibiting particularly high adsorption capacities. Compared with the other MRs, the nonpolar MRs X-5, HPD100, HPD300, and HP-20 presented greater adsorption/desorption capacities for ATF. A comparison of the physical properties of the MRs in Table S1 reveals that HPD300 resin has the smallest average pore size and the largest specific surface area, and exhibits superior adsorption and desorption capacity compared with the other MRs (Guo et al., 2015). The specific surface areas of X-5 and HPD100 are comparable; however, X-5 exhibits a larger average pore size and a stronger affinity for adsorbate molecules, potentially resulting in a diminished desorption capacity relative to that of HPD100, HPD300, and HP-20. Furthermore, the market prices of X-5, HPD100, HPD300 and HP-20 are comparable, with HPD300 occupying a middle position. HPD300 is a macroporous resin that has been widely used in industry and is distinguished by a long service life, which allows it to sustain satisfactory adsorption outcomes after two or three regenerations. Ultimately, HPD300 displays the most robust combined adsorption/desorption capacity and potential for practical large-scale applications, thus qualifying it as a candidate for the separation and purification of ATF.

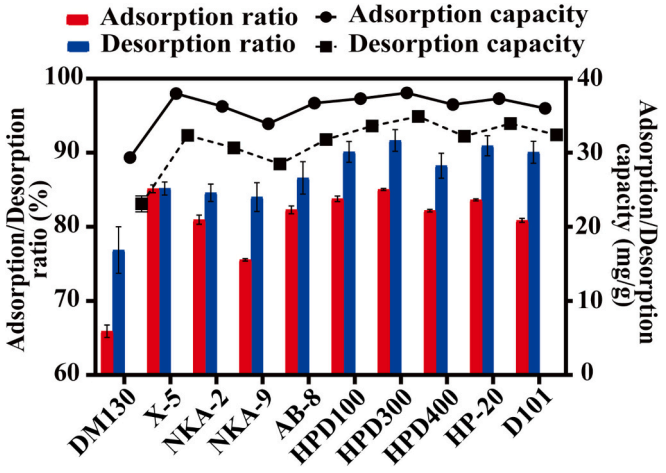

Fig. 3. Comparison of the adsorption and desorption performances of ten MRs.

3.2.2. Adsorption kinetics

Adsorption kinetic studies were conducted on the four MRs (X-5, HPD100, HPD300 and HP-20) with stronger adsorption properties. As shown in Fig. S2A, the quantities of the different MRs all increased with adsorption time. The adsorption capacity of ATF on the MRs rapidly increased during the initial 120 min, with the adsorption curves gradually becoming smooth after 360 min. Upon reaching equilibrium, the adsorption rate of HPD300 was the highest, followed by X-5, HPD100 and HP-20. This phenomenon might be attributed to HPD300 having the largest specific surface area, thereby allowing ATF to bind to a greater number of adsorption sites (Wang & Guo, 2020).

The adsorption mechanism of different MRs on ATF was described using the pseudo-first-order and pseudo-second-order models. As shown in Figs. S2B and S2C, the linear fit of the pseudo-second-order model exhibited a greater degree of accuracy than that of the pseudo-first-order model. As evidenced by the regression coefficient R^2, the pseudo-second-order model demonstrated a markedly superior fit compared with the pseudo-first-order model (Table 2). Additionally, the theoretical maximum adsorption capacity, $Q_{e(cal)}$, of the pseudo-second-order model was found to be more closely aligned with the experimental value, $Q_{e(exp)}$, than that of the pseudo-first-order model, $Q_{e(cal)}$. It could be concluded that the pseudo-second-order kinetic model was more

Table 2
Equations and parameters of the kinetic model.

Model	MRs	Kinetic Equation	Parameters			
			R^2	k_1	$Q_{e(cal)}$	$Q_{e(exp)}$
The pseudo-first-order model	X-5	$\ln(Q_e-Q_t) = -0.0041\ t + 2.6880$	0.7480	0.0041	14.70	38.46
	HPD100	$\ln(Q_e-Q_t) = -0.0041\ t + 2.7760$	0.8242	0.0041	16.05	37.54
	HPD300	$\ln(Q_e-Q_t) = -0.0037\ t + 2.9880$	0.7880	0.0037	19.85	39.58
	HP-20	$\ln(Q_e-Q_t) = -0.0039\ t + 2.8180$	0.7918	0.0039	16.74	36.76
			R^2	k_2	$Qe_{(cal)}$	$Qe_{(exp)}$
The pseudo-second-order model	X-5	$t/Q_t = 0.0249\ t + 0.6605$	0.9996	0.0009	40.24	38.46
	HPD100	$t/Q_t = 0.0256\ t + 0.7757$	0.9999	0.0008	39.11	37.54
	HPD300	$t/Q_t = 0.0236\ t + 1.0004$	0.9993	0.0006	42.32	39.58
	HP-20	$t/Q_t = 0.0258\ t + 0.8959$	0.9997	0.0007	38.77	36.76
			R^2	k_3	M	
Intraparticle diffusion model	X-5	$Q_t = 1.257\ t^{1/2} + 13.57$	0.712	1.2571	13.57	
	HPD100	$Q_t = 1.194\ t^{1/2} + 13.16$	0.7389	1.1944	13.16	
	HPD300	$Q_t = 1.413\ t^{1/2} + 10.75$	0.7800	1.4131	10.75	
	HP-20	$Q_t = 1.247\ t^{1/2} + 11.45$	0.7634	1.2472	11.45	

suitable for describing the adsorption of ATF by X-5, HPD100, HPD300, and HP-20. These results indicated that the adsorption of ATF by HPD300 occurred as a multilayer adsorption process.

To ascertain whether internal diffusion represented the limiting step in the adsorption rate, the intraparticle diffusion model was employed for the purpose of fitting the adsorption data (Wu et al., 2009). As shown in Fig. S2D, the fitted curve of Q_t versus $t_{1/2}$ exhibited a three-segment linear relationship, indicating that three successive steps regulated the adsorption process (Boparai et al., 2011). Furthermore, the curves generated by X-5, HPD100, HPD300, and HP-20 did not pass through the origin ($M \neq 0$), indicating that the rate-limiting step was not only intraparticle diffusion but also boundary layer diffusion during the adsorption process (Shin & Kim, 2016). HPD300 exhibited the highest rate constant ($k_3 = 1.4131$), indicating that ATF diffused more readily within this resin than in the other resins, resulting in a faster rate of adsorption of ATF. The adsorption process was faster and more efficient, reflecting the advantages of adsorption by HPD300. In summary, HPD300 was the most suitable resin for ATF adsorption.

3.2.3. Adsorption isotherms and thermodynamics

As depicted in Fig. 4A, under adsorption conditions of 25 °C, 35 °C, and 45 °C, the adsorption capacity of the same concentration of ATF on the HPD300 resin exhibited a sequential decline, indicating that an increase in temperature was detrimental to the adsorption of ATF on the HPD300 resin. Both the Langmuir and Freundlich models demonstrated a superior ability to describe the adsorption process of HPD300 on ATF (Figs. 4B-4C). However, the linear correlation coefficient R^2 of the Freundlich model was greater than that of the Langmuir model (Table 3). These findings implied that the Freundlich model was more appropriate for elucidating the adsorption process of ATF by HPD300.

As shown in Table 3, the k_L value decreased from 0.2528 to 0.2389 mL/mg, whereas the k_F value decreased from 2.3579 to 2.1891 mL/mg when the adsorption temperature increased from 25 to 45 °C. The adsorption of ATF by HPD300 is a nonspontaneous exothermic process, and high temperatures are detrimental to the adsorption of the HPD300 resin (Shen et al., 2022). In this study, the *1/n* values at 25, 35, and 45 °C were observed to be within the range of 0.1 to 0.5, indicating that the adsorption process of ATF by HPD300 was spontaneous within this temperature range. However, an increase in temperature from 25 to

Table 3
Adsorption isotherm model fitting to regression equations and adsorption parameters at different temperatures.

Model	T/(°C)	Equations	Parameters		
			R^2	k_L	Q_m
Langmuir	25	$C_e/Q_e = 0.0112C_e+0.0441$	0.8218	0.2528	89.61
	35	$C_e/Q_e = 0.0114C_e+0.0483$	0.9851	0.2363	87.64
	45	$C_e/Q_e = 0.0127C_e+0.0530$	0.9619	0.2389	78.99
			R^2	k_F	1/n
Freundlich	25	$\ln Q_e = 0.4241\ln C_e+3.0770$	0.9786	21.6932	0.4241
	35	$\ln Q_e = 0.4570\ln C_e+2.9890$	0.9979	19.8658	0.4570
	45	$\ln Q_e = 0.4568\ln C_e+2.8940$	0.9946	18.0654	0.4568

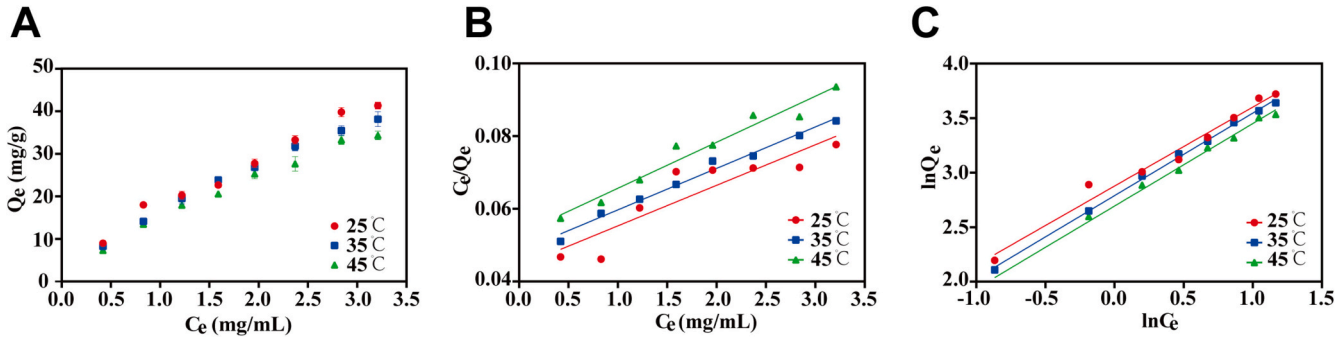

Fig. 4. (A) Adsorption isothermal curves, (B) Langmuir model, and (C) Freundlich model for the purification of ATF on HPD300 at temperatures of 25 °C, 35 °C, and 45 °C.

45 °C resulted in a corresponding increase in the *1/n* value, indicating a gradual hardening of the adsorption process. Overall, an adsorption temperature of 25 °C was more suitable for the purification of ATF by HPD300.

3.2.4. Optimization of the process conditions for ATF preparation by HPD300

The adsorption ability of HPD300 was found to be significantly influenced by the concentration of ATF. As shown in Fig. 5A, the adsorption capacity of HPD300 gradually increased with increasing concentration, whereas the adsorption rate reversed. Upon reaching a concentration of 2.79 mg/mL, the flavonoid molecules were observed to occupy the unabsorbed sites on HPD300, resulting in a gradual slowing of the increase in adsorption capacity and a concomitant decrease in the adsorption rate (Wang et al., 2022).

The pH value can influence the surface charge characteristics of the MRs and the degree of ionization of the adsorbed molecules, thereby determining the strength of the resin's adsorption capacity (Yang et al., 2024). As shown in Fig. 5B, the pH of the sample significantly influenced the performance of HPD300. The results demonstrated that a lower pH value (1.0–3.0) resulted in a better adsorption capacity than a higher pH value (6.0–8.0). This phenomenon might be attributed to the reduced interaction between HPD300 and ATF at higher pH values (Wang & Wang, 2019). At a pH value of 2.0, the HPD300 resin exhibited the greatest adsorption rate and adsorption capacity of 83.64 % and 49.24 mg/g, respectively.

The application of an appropriate resin–liquid ratio was conducive to purification. As the sample volume increased, the adsorption of ATF by HPD300 gradually increased, as shown in Fig. 5C, reaching a plateau at a resin–liquid ratio of 1:20. In contrast, the adsorption rate exhibited an inverse trend. When the quantity of resin is considerable, the resin adsorbs the majority of the flavonoid molecules present in the sample solution, resulting in a relatively high adsorption rate; conversely, the average number of flavonoid molecules adsorbed per resin particle is relatively low, resulting in a reduced adsorption capacity (Hou et al., 2019). In summary, the sample concentration was determined to be 2.79 mg/mL, the pH value was set at 2.0, and the resin–liquid ratio was established at 1:20.

In addition, the impact of elution conditions on ATF purification was also investigated. Given the disparate chemical properties of flavonoids with varying structures and states of existence, separate 0 % to 100 % ethanol solutions (*v*/v) were prepared for elution, with each ethanol concentration eluted until colorless. As illustrated in Fig. 5D, an increase in the elution flow rate resulted in a more asymmetrical change in the flavonoid content curve and greater consumption of ethanol (Xie et al., 2016). A flow rate of 3 BV/h resulted in the consumption of approximately 2 to 3 BV more ethanol than 0.75 BV/h and 1.5 BV/h. Although 0.75 BV/h consumed the least amount of ethanol, it required the longest elution time, approximately two to four times longer than the 1.5 BV/h and 3 BV/h flow rates. The elution of flavonoids from HP300 was largely achieved with a solution of 0 % to 50 % ethanol. Consequently, the concentration of flavonoids in the eluate was determined, and the percentage of flavonoids was calculated, as illustrated in Fig. 5E. The flavonoid contents of the fractions eluted at 1.5 BV/h were all above 50 %, with the highest contents observed in the fractions eluted with 20 % and 30 % ethanol, at 91.42 % and 90.68 %, respectively. Accordingly, the optimal elution flow rate was identified as 1.5 BV/h, and the requisite volumes for the ethanol concentration range of 0 % to 50 % were 2.3 BV, 6.7 BV, 16.7 BV, 14.3 BV, 8.5 BV, and 3.3 BV, respectively. In the preceding study, the flavonoid content of *Euphorbia hirta* L. purified with HPD-300 resin increased from 6.32 % to 28.8 % (Wen Y., Liu M., & Mai X., 2023). In comparison, the ATF content increased significantly from 21.71 % to more than 90 % before and after isolation and purification in the present study. These findings indicated that the HPD-300 resin was effective for isolating and purifying ATF.

The impacts of sample concentration (A), pH (B), and the resin–liquid ratio (C) on the adsorption rates/capacities were investigated. Additionally, the influence of flow rates on changes in volume required (BV) and the ATF content (mg) under elution conditions (D), wherein each ethanol gradient was eluted to colorless, was examined. Finally, the flavonoid content was evaluated by elution from 0 % to 50 % ethanol (E).

3.3. Antioxidant and hypoglycemic activities

As shown in Figs. 6A to 6D, the radical scavenging capacity and iron

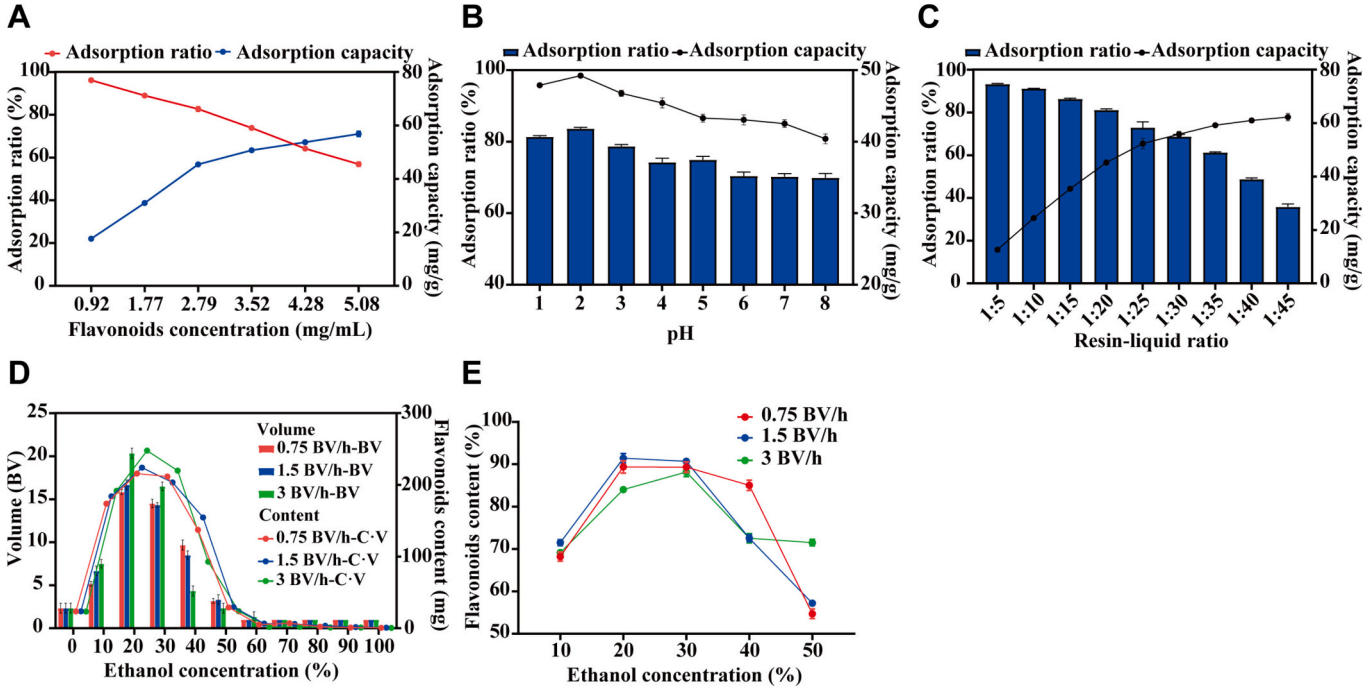

Fig. 5. Optimization of adsorption/desorption conditions for the purification of ATF by HPD300.

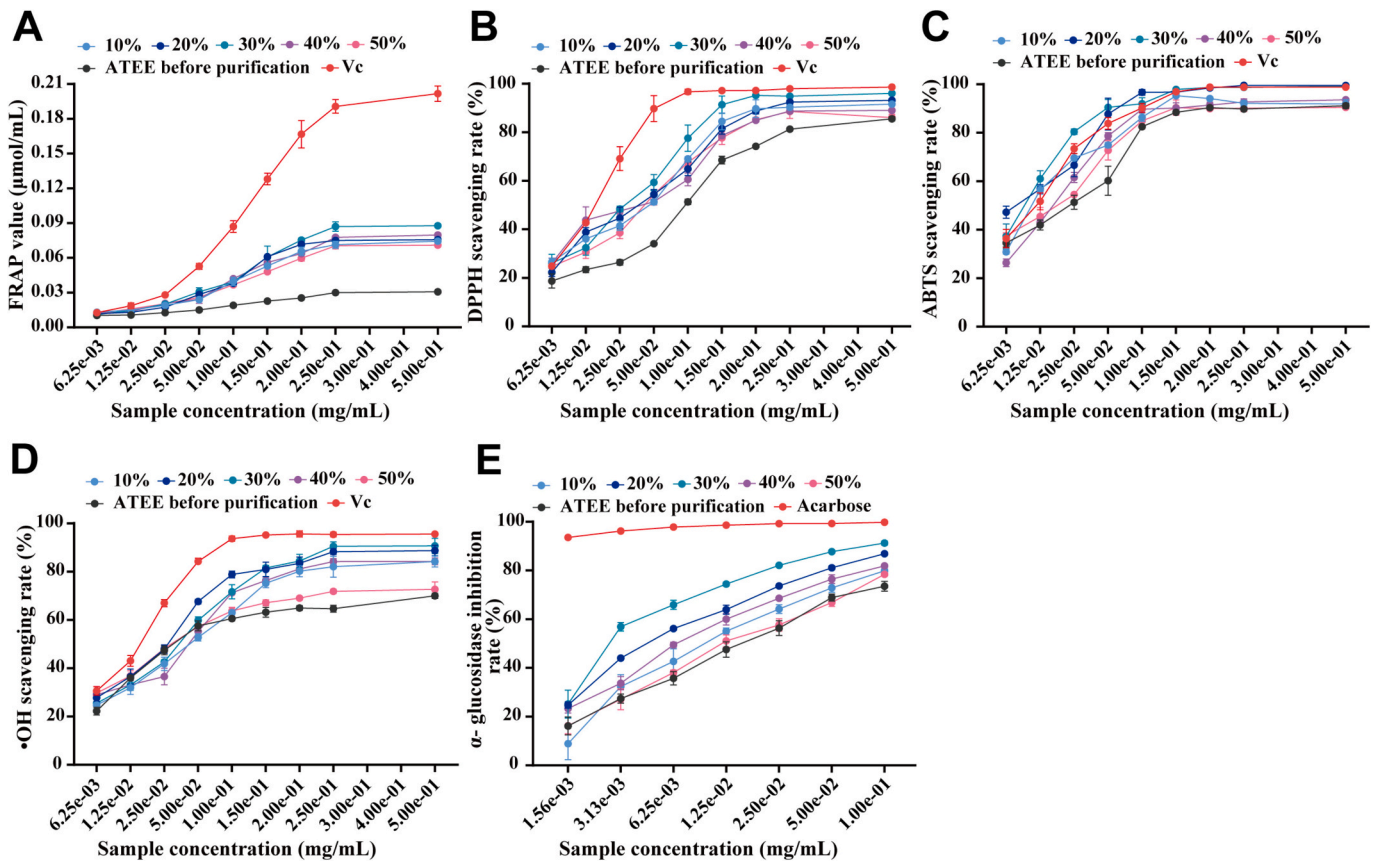

Fig. 6. Radical scavenging activity and α-glycosidase inhibitory activity of different ethanol elutions and ATEE before purification.

ion reduction capacity were positively correlated with increasing concentrations of flavonoids. In this instance, the antioxidant capacity of the 30 % ethanol elution mixture was found to be greater than that of Vc, followed by the 20 % ethanol elution mixture, whereas the crude extract and 50 % ethanol elution mixture presented a weaker antioxidant capacity. This findings might be associated with the distinct contents and chemical compositions of flavonoids in various concentrations of ethanol (Cui et al., 2022). Furthermore, a comparison of the IC_{50} values for DPPH, ABTS, and ·OH in Table 4 revealed that the antioxidant capacity of the fraction followed the order of 30 % > 20 % > 40 % > 10 % > 50 % > ATEE. The antioxidant capacities of the 20 % and 30 % fractions were greater than those of the other fractions.

The inhibition of α-glucosidase activity by each elution mixture is plotted in Fig. 6E. The 30 % ethanol mixture demonstrated the most potent inhibitory effect on α-glucosidase activity. The IC_{50} values of each elution in the α-glucosidase reaction system were calculated separately (Table 4), revealing that the inhibitory effect on α-glucosidase activity was strongest in the 30 % ethanol mixture, followed by the 20 % ethanol mixture, 40 %, 10 %, and 50 % ethanol mixture, and finally ATEE. These results were consistent with the flavonoid content observed in each ethanol elution and the results of the antioxidant activity determination, indicating that 20 % and 30 % ethanol might represent the optimal elution dose for the purification of flavonoids in AT by HPD300. Consequently, 20 % and 30 % ethanol elution could be employed in future investigations of ATF.

Table 4
IC_{50} values for DPPH, ABTS, hydroxyl radical, and α-glucosidase.

Sample	DPPH(mg/mL)	ABTS(mg/mL)	·OH(mg/mL)	α-glucosidase(U/mL)
ATEE	0.0710	0.0190	0.0456	0.0161
10 %	0.0304	0.0118	0.0372	0.0113
20 %	0.0298	0.0086	0.0233	0.0054
30 %	0.0251	0.0090	0.0294	0.0034
40 %	0.0282	0.0161	0.0337	0.0078
50 %	0.0354	0.0148	0.0339	0.0144

(A) FRAP values; (B) DPPH, (C) ABTS, and (D) hydroxyl radical scavenging rate; (E) α-glucosidase inhibition rate. The ATF-rich fractions were obtained by eluting with different concentrations of ethanol (10 %, 20 %, 30 %, 40 % and 50 %).

3.4. Phytochemical analysis of the purified ATF

Given that the 20 % and 30 % ethanol-eluting fractions had higher flavonoid contents (>90 %, Fig. 7A) and better biological activities, we analyzed the phytochemical compositions of the mixtures of the 20 % and 30 % ethanol-eluting fractions using plant-wide targeted metabolomics. A total of 1257 compounds were identified, which could be broadly categorized into flavonoids, polyphenols, alkaloids, phytohormones, terpenoids, benzenes, keto acids, fatty acyls, vitamins, nucleotides, and others (Fig. 7B and C). Flavonoids presented the highest relative abundance (73.83 %) and were primarily composed of (+)-epicatechin (24.94 %), isoquercitrin (14.02 %), astragalin (7.66 %), kaempferol-3-O-rutinoside (6.84 %), procyanidin B2 (5.51 %), and other substances (Fig. 7D, Table S4).

Flavonoids are a class of active substances that play important roles in traditional Chinese medicine and phytochemistry. They have been shown to possess a range of beneficial properties, including antioxidant, antibacterial, anti-cell degeneration, anticancer, hypoglycemic and hypolipidemic effects. Flavonoids are employed as the primary active ingredients in a range of existing functional products, including propolis (Irigoiti et al., 2021), bee bread (Aksoy et al., 2024) and soy products (Hu et al., 2020), with the objective of promoting health. Among these epicatechin (Jug et al., 2021), isoquercitrin (Heřmánková-Vavříková

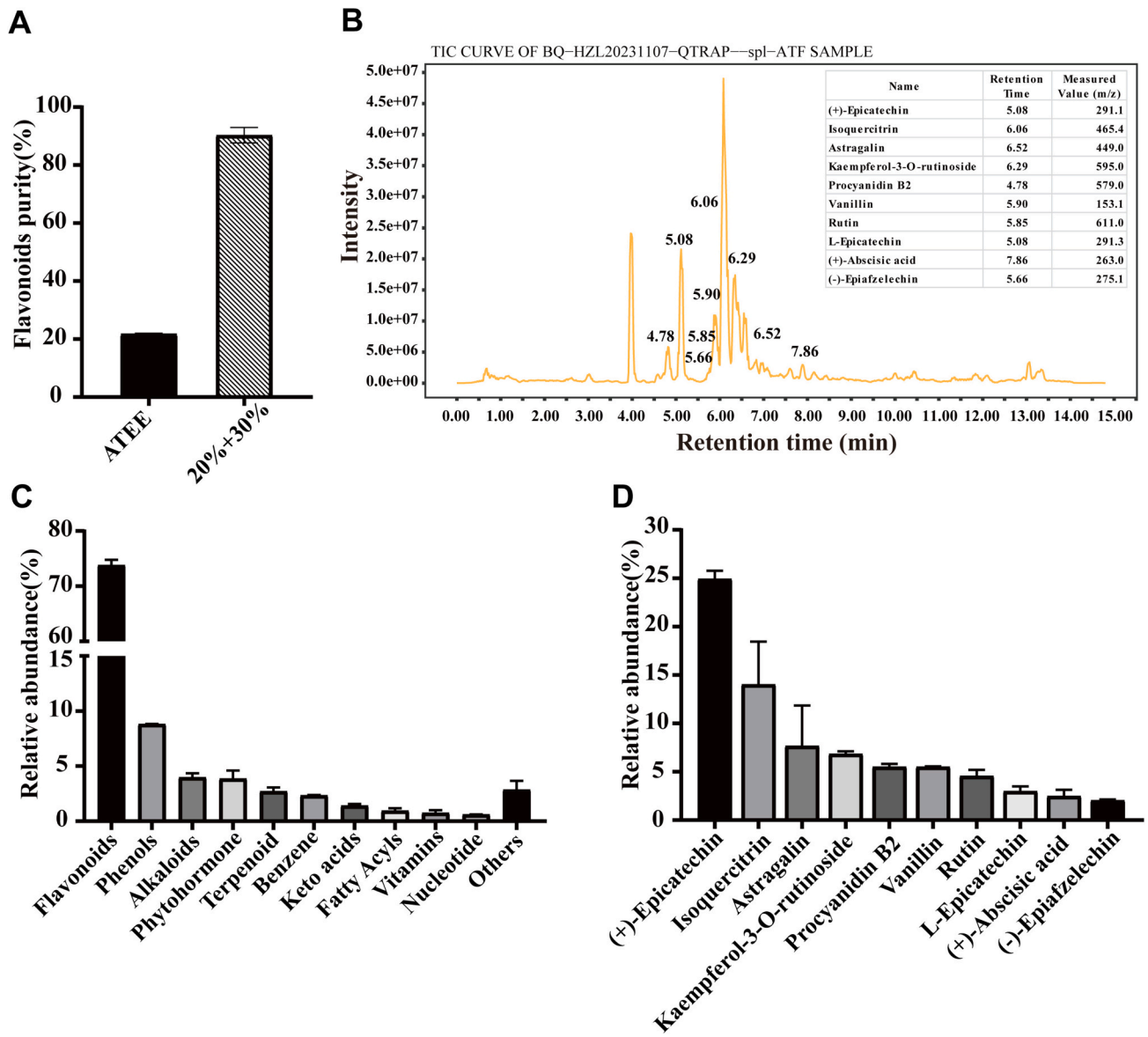

Fig. 7. The main chemical components of ATF based on widely targeted metabolomics.

et al., 2017) and astragalin (Li et al., 2017) have been reported to possess effective free radical scavenging properties, likely due to the high number of hydroxyl groups present in their molecular structures (Nagarajan et al., 2020). Quercetin, rutin and catechin have high reducing capacities for ferric ions and inhibit hemolysis caused by high Fe^{2+} concentrations (Cherrak et al., 2016). In addition, epicatechin, kaempferol-3-O-rutinoside and rutin significantly inhibit α-glucosidase (Calzada et al., 2017; Hua et al., 2021; Uysal et al., 2016). Flavanols, flavonols and isoflavones reduce the risk of T2DM (Yi et al., 2023). Furthermore, investigation of the pharmacological activities of AT showed that flavonoid molecules are effective in alleviating the symptoms of loperamide-induced functional constipation, exhibiting superior anti-inflammatory efficacy (Hu et al., 2023). Concurrently, catechin and epicatechin, extracted from the AT, were observed to markedly inhibit the production of NO in mouse RAW 264.7 cells (Choi et al., 2018). The findings of these previous studies not only validated the results of the present study regarding the in vitro antioxidant and hypoglycemic activities of ATF but also indicated that further research and development of ATF are warranted.

(A) Flavonoid content before (ATEE) and after purification (mixture of 20 % and 30 % ethanol elution); (B) TIC plots of 20 % and 30 % ethanol elution mixture, with the top ten compounds noted in the figure; (C) the top 10 classifications; and (D) the relative abundance of the top ten compounds. Data are expressed as the means ± SEMs ($n = 3$).

4. Conclusion

In this work, we developed an efficient method for the extraction and purification of ATF, as well as an in vitro evaluation of the antioxidant and α-glucosidase inhibitory activities of ATF extracts. The optimal extraction conditions were determined to be ethanol concentration of 60 %, a material-to-liquid ratio of 1:39 (*w/v*), and ultrasonic power, time, and temperature of 160 W, 47 min, and 69 °C, respectively. The flavonoid yield of ATEE reached 3.33 %. The purification of ATF via HPD300 was more efficient than that of the other MRs. Furthermore, its adsorption isotherm was found to conform to the Freundlich adsorption model. Under the optimized HPD300 adsorption conditions, different fractions with relatively high flavonoid contents could be separated using different concentrations (0 % to 50 %) of ethanol for elution. The flavonoid contents of the 20 % and 30 % ethanol elutions were greater than 90 %, indicating enhanced antioxidant and α-glucosidase inhibition abilities. The 20 % and 30 % ethanol elutions contained mainly

flavonoids such as epicatechin, isoquercitrin, echinacoside, kaempferol-3-O-rutinoside, proanthocyanidin B2, and rutin. These findings provide a theoretical basis for the efficient preparation of ATF and the in-depth development and utilization of AT resources.

CRediT authorship contribution statement

Zelin Huang: Writing – original draft, Visualization, Validation, Software, Methodology, Investigation, Data curation. **Yan Zhao:** Writing – original draft, Validation, Supervision, Software, Methodology, Investigation, Funding acquisition. **Weixing Yang:** Methodology, Data curation. **Lu Lang:** Investigation, Data curation. **Jun Sheng:** Supervision, Resources. **Yang Tian:** Writing – review & editing, Supervision, Software, Methodology, Funding acquisition, Data curation. **Xiaoyu Gao:** Writing – review & editing, Supervision, Resources, Investigation, Funding acquisition, Conceptualization.

Declaration of competing interest

The authors declare that they have no known competing financial interests or personal relationships that could have appeared to influence the work reported in this paper.

Acknowledgment

This research was funded by the Xingdian talent plan of Yunnan Province (Young Talents Project, 2022-0255), the scientific research fund of Yunnan Provincial Department of Education (2024J0478) and the Yunnan Province-City Integration Project (202302AN360002).

Appendix A. Supplementary data

Supplementary data to this article can be found online at https://doi.org/10.1016/j.fochx.2025.102177.

Data availability

Data will be made available on request.

References

Aksoy, A., Altunatmaz, S. S., Aksu, F., Tokatlı Demirok, N., Yazıcı, K., & Yıkmış, S. (2024). Bee bread as a functional product: Phenolic compounds, amino acid, sugar, and organic acid profiles. *Foods (Basel, Switzerland), 13*(5), 795. https://doi.org/10.3390/foods13050795

Andrade, A. W. L., Machado, K. D. C., Machado, K. D. C., Figueiredo, D. D. R., David, J. M., Islam, M. T., & Costa, J. P. (2018). In vitro antioxidant properties of the biflavonoid agathisflavone. *Chemistry Central Journal, 12*(1), 75. https://doi.org/10.1186/s13065-018-0443-0

Boparai, H. K., Joseph, M., & O'Carroll, D. M. (2011). Kinetics and thermodynamics of cadmium ion removal by adsorption onto nano zerovalent iron particles. *Journal of Hazardous Materials, 186*(1), 458–465. https://doi.org/10.1016/j.jhazmat.2010.11.029

Cai, R., Yue, X., Wang, Y., Yang, Y., Sun, D., Li, H., & Chen, L. (2021). Chemistry and bioactivity of plants from the genus *Amomum*. *Journal of Ethnopharmacology, 281*, Article 114563. https://doi.org/10.1016/j.jep.2021.114563

Calzada, F., Solares-Pascasio, J. I., Ordoñez-Razo, R. M., Velazquez, C., Barbosa, E., García-Hernández, N., & Correa-Basurto, J. (2017). Antihyperglycemic activity of the leaves from *Annona cherimola* miller and rutin on alloxan-induced diabetic rats. *Pharmacognosy Research, 9*(1), 1–6. https://doi.org/10.4103/0974-8490.199781

Chávez-González, M. L., Sepúlveda, L., Verma, D. K., Luna-García, H. A., Rodríguez-Durán, L. V., Ilina, A., & Aguilar, C. N. (2020). Conventional and emerging extraction processes of flavonoids. *Processes, 8*(4), 434. https://doi.org/10.3390/pr8040434

Cherrak, S. A., Mokhtari-Soulimane, N., Berroukeche, F., Bensenane, B., Cherbonnel, A., Merzouk, H., & Elhabiri, M. (2016). In vitro antioxidant versus metal ion chelating properties of flavonoids: A structure-activity investigation. *PLoS One, 11*(10), Article e0165575. https://doi.org/10.1371/journal.pone.0165575

Choi, C. W., Shin, J. Y., Seo, C., Hong, S. S., Ahn, E. K., Jung, Y. H., & Oh, J. S. (2018). In vitro anti-inflammatory activity of the components of amomum tsao-ko in murine macrophage raw 264.7 cells. *African Journal of Traditional, Complementary and Alternative Medicines, 15*(2), 26–34. https://doi.org/10.21010/AJTCAMV15I2.4

Cui, L., Ma, Z., Wang, D., & Niu, Y. (2022). Ultrasound-assisted extraction, optimization, isolation, and antioxidant activity analysis of flavonoids from *Astragalus membranaceus* stems and leaves. *Ultrasonics Sonochemistry, 90*, Article 106190. https://doi.org/10.1016/j.ultsonch.2022.106190

Dao, T. B., Nguyen, T. M., Nguyen, V. Q., Tran, T. M., Tran, N. M., Nguyen, C. H., & Duong, T. H. (2021). Flavones from *Combretum quadrangulare* growing in Vietnam and their alpha-glucosidase inhibitory activity. *Molecules, 26*(9), 2531. https://doi.org/10.3390/molecules26092531

Guo, H. D., Zhang, Q. F., Chen, J. G., Shangguang, X. C., & Guo, Y. X. (2015). Large scale purification of puerarin from Puerariae Lobatae Radix through resins adsorption and acid hydrolysis. *Journal of Chromatography. B, Analytical Technologies in the Biomedical and Life Sciences, 980*, 8–15. https://doi.org/10.1016/j.jchromb.2014.12.014

Heřmánková-Vavříková, E., Křenková, A., Petrásková, L., Chambers, C. S., Zápal, J., Kuzma, M., & Křen, V. (2017). Synthesis and antiradical activity of isoquercitrin esters with aromatic acids and their homologues. *International Journal of Molecular Sciences, 18*(5), 1074. https://doi.org/10.3390/ijms18051074

Hou, M., Hu, W., Xiu, Z., Jiang, A., Men, L., Hao, K., & Cao, D. (2019). Preparative purification of total flavonoids from *Sophora tonkinensis* Gagnep. By macroporous resin column chromatography and comparative analysis of flavonoid profiles by HPLC-PAD. *Molecules, 24*(17). https://doi.org/10.3390/molecules24173200

Hu, C., Wong, W. T., Wu, R., & Lai, W. F. (2020). Biochemistry and use of soybean isoflavones in functional food development. *Critical Reviews in Food Science and Nutrition, 60*(12), 2098–2112. https://doi.org/10.1080/10408398.2019.1630598

Hu, Y., Gao, X., Zhao, Y., Liu, S., Luo, K., Fu, X., … Fan, Y. (2023). Flavonoids in *Amomum tsaoko Crevost et Lemarie* ameliorate loperamide-induced constipation in mice by regulating gutmicrobiota and relatedmetabolites. *International Journal of Molecular Sciences, 24*(8), 7191. https://doi.org/10.3390/ijms24087191

Hua, F., Zhou, P., Liu, P. P., & Bao, G. H. (2021). Rat plasma protein binding of kaempferol-3-O-rutinoside from Lu'an GuaPian tea and its anti-inflammatory mechanism for cardiovascular protection. *Journal of Food Biochemistry, 45*(7), Article e13749. https://doi.org/10.1111/jfbc.13749

Irigoiti, Y., Navarro, A., Yamul, D., Libonatti, C., Tabera, A., & Basualdo, M. (2021). The use of propolis as a functional food ingredient: A review. *Trends in Food Science & Technology, 115*, 297–306. https://doi.org/10.1016/j.tifs.2021.06.041

Jug, U., Naumoska, K., & Vovk, I. (2021). (−)-Epicatechin-an important contributor to the antioxidant activity of Japanese knotweed rhizome bark extract as determined by antioxidant activity-guided fractionation. *Antioxidants (Basel), 10*(1), 133. https://doi.org/10.3390/antiox10010133

Li, H., Lin, J., Bai, B., Bo, T., He, Y., Fan, S., & Zhang, J. (2023). Study on purification, identification and antioxidant of flavonoids extracted from perilla leaves. *Molecules (Basel, Switzerland), 28*(21), 7273. https://doi.org/10.3390/molecules28217273

Li, H., Yang, J., Wang, M., Ma, X., & Peng, X. (2023). Studies on the inhibition of α-glucosidase by biflavonoids and their interaction mechanisms. *Food Chemistry, 420*, Article 136113. https://doi.org/10.1016/j.foodchem.2023.136113

Li, J., & Chase, H. A. (2010). Development of adsorptive (non-ionic) macroporous resins and their uses in the purification of pharmacologically-active natural products from plant sources. *Natural Product Reports, 27*(10), 1493–1510. https://doi.org/10.1039/c0np00015a

Li, X., Tian, Y., Wang, T., Lin, Q., Feng, X., Jiang, Q., & Chen, D. (2017). Role of the p-Coumaroyl moiety in the antioxidant and cytoprotective effects of flavonoid glycosides: Comparison of astragalin and tiliroside. *Molecules, 22*(7), 1165. https://doi.org/10.3390/molecules22071165

Liao, J., Guo, Z., & Yu, G. (2021). Process intensification and kinetic studies of ultrasound-assisted extraction of flavonoids from peanut shells. *Ultrasonics Sonochemistry, 76*, Article 105661. https://doi.org/10.1016/j.ultsonch.2021.105661

Lin, Y., Lu, M. F., Liao, H. B., Li, Y. X., Han, W., & Yuan, K. (2014). Content determination of the flavonoids in the different parts and different species of *Abelmoschus esculentus* L. by reversed phase-high performance liquid chromatograph and colorimetric method. *Pharmacognosy Magazine, 10*(39), 278–284. https://doi.org/10.4103/0973-1296.137368

Maduwanthi, S. D. T., & Marapana, R. (2021). Total phenolics, flavonoids and antioxidant activity following simulated gastro-intestinal digestion and dialysis of banana (*Musa acuminata*, AAB) as affected by induced ripening agents. *Food Chemistry, 339*, Article 127909. https://doi.org/10.1016/j.foodchem.2020.127909

Nagarajan, S., Nagarajan, R., Kumar, J., Salemme, A., Togna, A. R., Saso, L., & Bruno, F. (2020). Antioxidant activity of synthetic polymers of phenolic compounds. *Polymers (Basel), 12*(8), 1646. https://doi.org/10.3390/polym12081646

Qin, G., Zhang, F., Ren, M., Chen, X., Liu, C., Li, G., … Wang, G. (2023). Eco-friendly and efficient extraction of polyphenols from Ligustrum robustum by deep eutectic solvent assisted ultrasound. *Food Chemistry, 429*, Article 136828. https://doi.org/10.1016/j.foodchem.2023.136828

Shen, D., Labreche, F., Wu, C., Fan, G., Li, T., Dou, J., & Zhu, J. (2022). Ultrasound-assisted adsorption/desorption of jujube peel flavonoids using macroporous resins. *Food Chemistry, 368*, Article 130800. https://doi.org/10.1016/j.foodchem.2021.130800

Shin, H. S., & Kim, J. H. (2016). Isotherm, kinetic and thermodynamic characteristics of adsorption of paclitaxel onto Diaion HP-20. *Process Biochemistry, 51*(7), 917–924. https://doi.org/10.1016/j.procbio.2016.03.013

Teng, X., Zhang, M., & Devahastin, S. (2019). New developments on ultrasound-assisted processing and flavor detection of spices: A review. *Ultrasonics Sonochemistry, 55*, 297–307. https://doi.org/10.1016/j.ultsonch.2019.01.014

Tian, J., Muhammad, S., Chen, A., Chen, P., Wang, J., Yang, C., & Wang, Z. (2019). An experimental study exploring the influencing factors for ultrasonic-assisted extraction of flavonoid compounds from leaves of Amorpha fruticosa L. *Journal of Forestry Research, 30*(5), 1735–1741. https://doi.org/10.1007/s11676-019-00931-y

Uysal, A., Zengin, G., Mollica, A., Gunes, E., Locatelli, M., Yilmaz, T., & Aktumsek, A. (2016). Chemical and biological insights on *Cotoneaster integerrimus*: A new (−)-

epicatechin source for food and medicinal applications. *Phytomedicine, 23*(10), 979–988. https://doi.org/10.1016/j.phymed.2016.06.011

Vo, T. P., Pham, N. D., Pham, T. V., Nguyen, H. Y., Vo, L. T. V., Tran, T. N. H., & Nguyen, D. Q. (2023). Green extraction of total phenolic and flavonoid contents from mangosteen (*Garcinia mangostana* L) rind using natural deep eutectic solvents. *Heliyon, 9*(4), Article e14884. https://doi.org/10.1016/j.heliyon.2023.e14884

Wang, J., & Guo, X. (2020). Adsorption kinetic models: Physical meanings, applications, and solving methods. *Journal of Hazardous Materials, 390*, Article 122156. https://doi.org/10.1016/j.jhazmat.2020.122156

Wang, X. H., & Wang, J. P. (2019). Effective extraction with deep eutectic solvents and enrichment by macroporous adsorption resin of flavonoids from *Carthamus tinctorius* L. *Journal of Pharmaceutical and Biomedical Analysis, 176*, Article 112804. https://doi.org/10.1016/j.jpba.2019.112804

Wang, Y., Zhang, Y., Cheng, J., Zhao, J., Shi, R., He, L., & Chen, Y. (2022). Efficient purification of flavonoids from bamboo shoot residues of Phyllostachys edulis by macroporous resin and their hypoglycemic activity. *Food Chem X, 16*, Article 100505. https://doi.org/10.1016/j.fochx.2022.100505

Wen, Y., Liu, M., & Mai, X. (2023). Optimisation of ultrasonic-assisted extraction and biological activity of total flavonoids from leaves of *Murrayae exotica* using response surface methodology. *Folia Horticulturae, 35*, 135–148. https://doi.org/10.2478/fhort-2023-0010

Wen, Y., Zeng, X., Dai, H., & Liu, B. (2023). Optimization of ultrasonic assisted extraction and biological activity of total flavonoids from *Ligusticum chuanxiong* Hort. Using response surface methodology. *Biomass Conversion and Biorefinery, 26*, 1–13. https://doi.org/10.1007/s13399-023-03832-7

Wu, F. C., Tseng, R. L., & Juang, R. S. (2009). Initial behavior of intraparticle diffusion model used in the description of adsorption kinetics. *Chemical Engineering Journal, 153*(1), 1–8. https://doi.org/10.1016/j.cej.2009.04.042

Wu, Y. J., Xin, R. H., & M., L., M., Z. Z., W., G., R., W., & P., L. Y.. (2023). Investigation on the changes of odor-active compounds of *Amomum tsao-ko* during natural drying. *Journal of Food Composition and Analysis, 122*, Article 105432. https://doi.org/10.1016/j.jfca.2023.105432

Xie, Y., Guo, Q. S., & Wang, G. S. (2016). Preparative separation and purification of the total flavonoids in *Scorzonera austriaca* with macroporous resins. *Molecules, 21*(6), 768. https://doi.org/10.3390/molecules21060768

Yang, S., Xue, Y., Chen, D., & Wang, Z. (2022). *Amomum tsao-ko* Crevost & Lemarié: A comprehensive review on traditional uses, botany, phytochemistry, and pharmacology. *Phytochemistry Reviews, 21*(5), 1487–1521. https://doi.org/10.1007/s11101-021-09793-x

Yang, Y., Liang, Q., Zhang, B., Zhang, J., Fan, L., Kang, J., & Ho, L. H. (2024). Adsorption and desorption characteristics of flavonoids from white tea using macroporous adsorption resin. *Journal of Chromatography. A, 1715*, Article 464621. https://doi.org/10.1016/j.chroma.2023.464621

Yi, X., Dong, M., Guo, N., Tian, J., Lei, P., Wang, S., & Shi, Y. (2023). Flavonoids improve type 2 diabetes mellitus and its complications: A review. *Frontiers in Nutrition, 10*, 1192131. https://doi.org/10.3389/fnut.2023.1192131

Zhang, T. T., Lu, C. L., & Jiang, J. G. (2014). Bioactivity evaluation of ingredients identified from the fruits of *Amomum tsaoko* Crevost et Lemaire, a Chinese spice. *Food & Function, 5*(8), 1747–1754. https://doi.org/10.1039/c4fo00169a

Zhang, X. F., Tang, Y. J., Guan, X. X., Lu, X., Li, J., Chen, X. L., & Fan, J. M. (2022). Flavonoid constituents of *Amomum tsao-ko* Crevost et Lemarie and their antioxidant and antidiabetic effects in diabetic rats - in vitro and in vivo studies. *Food & Function, 13*(1), 437–450. https://doi.org/10.1039/d1fo02974f